Current Biology 24, 2327–2334, October 6, 2014 ©2014 Elsevier Ltd All rights reserved http://dx.doi.org/10.1016/j.cub.2014.08.029

Report

A Unique Set of Centrosome Proteins Requires Pericentrin for Spindle-Pole Localization and Spindle Orientation

Chun-Ting Chen,[1,9,11] Heidi Hehnly,[1,8,9] Qing Yu,[2,9] Debby Farkas,[2] Guoqiang Zheng,[1] Sambra D. Redick,[1] Hui-Fang Hung,[1] Rajeev Samtani,[2] Agata Jurczyk,[1] Schahram Akbarian,[3,4] Carol Wise,[5] Andrew Jackson,[6] Michael Bober,[7] Yin Guo,[3] Cecilia Lo,[2,10] and Stephen Doxsey[1,10,*]

[1]Program in Molecular Medicine, University of Massachusetts Medical Center, Worcester, MA 01605, USA
[2]Department of Developmental Biology, University of Pittsburgh School of Medicine, Pittsburgh, PA 15261, USA
[3]Department of Psychiatry, University of Massachusetts Medical Center, Worcester, MA 01655, USA
[4]Departments of Psychiatry and Neuroscience, Mount Sinai School of Medicine, New York, NY 10029, USA
[5]Sarah M. and Charles E. Seay Center for Musculoskeletal Research, Texas Scottish Rite Hospital for Children, Dallas, TX 75219, USA
[6]MRC Human Genetics Unit, Institute of Genetics and Molecular Medicine, Western General Hospital, Edinburgh EH4 2XU, UK
[7]Division of Genetics, Department of Pediatrics, A.I. Dupont Hospital for Children, Wilmington, DE 19803, USA

Summary

Majewski osteodysplastic primordial dwarfism type II (MOPDII) is caused by mutations in the centrosome gene *pericentrin* (*PCNT*) that lead to severe pre- and postnatal growth retardation [1]. As in MOPDII patients, disruption of *pericentrin* (*Pcnt*) in mice caused a number of abnormalities including microcephaly, aberrant hemodynamics analyzed by in utero echocardiography, and cardiovascular anomalies; the latter being associated with mortality, as in the human condition [1]. To identify the mechanisms underlying these defects, we tested for changes in cell and molecular function. All $Pcnt^{-/-}$ mouse tissues and cells examined showed spindle misorientation. This mouse phenotype was associated with misdirected ventricular septal growth in the heart, decreased proliferative symmetric divisions in brain neural progenitors, and increased misoriented divisions in fibroblasts; the same phenotype was seen in fibroblasts from three MOPDII individuals. Misoriented spindles were associated with disrupted astral microtubules and near complete loss of a unique set of centrosome proteins from spindle poles (ninein, Cep215, centriolin). All these proteins appear to be crucial for microtubule anchoring and all interacted with Pcnt, suggesting that Pcnt serves as a molecular scaffold for this functionally linked set of spindle pole proteins. Importantly, *Pcnt* disruption had no detectable effect on localization of proteins involved in the cortical polarity pathway (NuMA, $p150^{glued}$, aPKC). Not only do these data reveal a spindle-pole-localized complex for spindle orientation, but they identify key spindle symmetry proteins involved in the pathogenesis of MOPDII.

Results and Discussion

The pathogenic mechanisms underlying the complex clinical features of the primordial dwarfism, Majewski osteodysplastic primordial dwarfism (MOPDII), are unclear. The cause of MOPDII is biallelic loss-of-function mutations in the centrosome gene, *pericentrin* (*PCNT*) [2], which lead to a loss of functional protein. MOPDII is characterized by severe intrauterine growth retardation progressing to microcephaly, bony dysplasia, and unusual facial features [3, 4]. MOPDII patients develop vascular abnormalities including vascular overgrowth and cardiovascular defects such as atrioventricular septal defects (AVSD). These vascular defects contribute to high morbidity and mortality secondary to cerebral aneurysms, stroke, and myocardial infarction [5]. Despite identification of the causative genetic mutation, a common mechanism for the multiorgan defects in MOPDII has not been elucidated.

To understand the cellular and molecular basis of MOPDII phenotypes, we engineered $Pcnt^{-/-}$ mice by insertional mutagenesis (Figure S1A available online). Mouse tissues, mouse embryonic fibroblasts (MEFs), and immortalized MEF lines confirmed loss of protein (Figures S1B–S1D and S3F) and mRNA (data not shown). Strikingly, $Pcnt^{-/-}$ mice exhibited many MOPDII features [2, 4–6] including small body size, microcephaly, craniofacial developmental anomalies (abnormal head shape, eye defects, and cleft palate) (Figures 1A and S2A–S2C), and structural kidney defects (Figures S2I and S2J). As in MOPDII, $Pcnt^{-/-}$ mice also developed vascular anomalies. These included structural and hemodynamic cardiovascular defects from E11.5 to E17.5, including head and whole-body hemorrhaging (Figures 1A and 1B), increased vascular density in head and abdomen (Figure 1C and data not shown), atrioventricular septal defects (Figure 1D), aberrant valve formation, and aortic blood collection from both ventricles (overriding aorta; for summary of related cardiac defects and other anomalies, see Table S1). These defects were associated with severe cardiac dysfunction. In utero ultrasound and spectral Doppler imaging of each individual embryo revealed mitral valve and aortic regurgitation (Figures 1E and 1F; n = 5/7 in 1E and n = 2/5 in 1F) and disrupted hemodynamics, leading to heart failure and prenatal lethality at E15.5 and E17.5. Similar cardiovascular anomalies are manifested in MOPDII and appear to be major contributors to death in both organisms.

To identify potential disease mechanisms, we first examined cellular and molecular functions associated with Pcnt during mitosis by using primary $Pcnt^{-/-}$ MEFs. The most prominent feature of mitotic spindles in $Pcnt^{-/-}$ MEFs was a dramatic reduction in astral microtubules (MTs) (Figure 2A, inset). We identified a ~4-fold decrease in both astral MT immunofluorescence intensity and MT length (Figures 2C and 2D). This phenotype is known to disrupt MT contacts with the cell cortex

[8]Present address: Department of Pharmacology, University of Washington School of Medicine, Seattle, WA 98103, USA
[9]Co-first author
[10]Co-senior author
[11]Died July 20, 2014
*Correspondence: stephen.doxsey@umassmed.edu

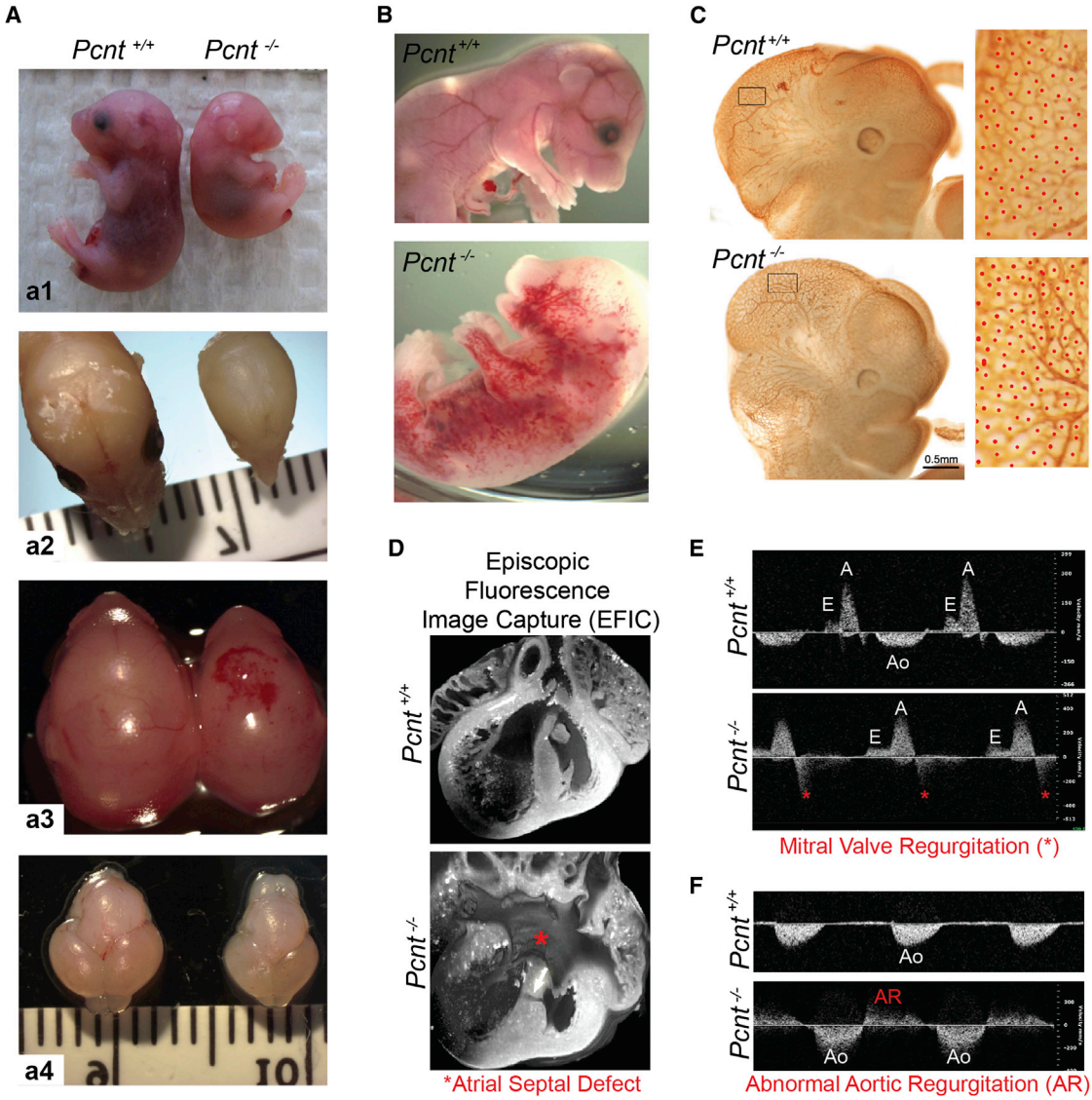

Figure 1. *Pcnt*$^{-/-}$ Mice Exhibit Growth Retardation, Microcephaly, Vascular Anomalies, and Structural Heart Defects

(A) *Pcnt*$^{-/-}$ mice exhibit intrauterine growth retardation (a1, 35% smaller, $p < 0.01$; >50 mice in 7 l); defects in cranial development (a2), intracranial hemorrhaging (a3), and microcephaly (a4).

(B) Representative images showing whole-body hemorrhaging in *Pcnt*$^{-/-}$ mouse (bottom) compared to the wild-type littermate (top).

(C) PECAM stain of vascular network in head of E11.5 *Pcnt*$^{+/+}$ (top row) and *Pcnt*$^{-/-}$ (bottom row) embryos. Boxed regions (left) are enlarged on the right, showing increased density of vascular plexuses (red dots) in *Pcnt*$^{-/-}$ head versus region-matched *Pcnt*$^{+/+}$ ($p < 0.0001$).

(D) Three-dimensional episcopic fluorescence image capture (EFIC) obtained from heart of E17.5 *Pcnt*$^{+/+}$ (top) and *Pcnt*$^{-/-}$ (bottom) mice reveal defective septum formation (asterisk) in *Pcnt*$^{-/-}$ neonates in contrast to the *Pcnt*$^{+/+}$ littermate.

(E and F) Doppler echocardiography reveals structural heart defects and congestive heart failure in *Pcnt*$^{-/-}$ embryos (bottom) but not in *Pcnt*$^{+/+}$ littermates (top), as indicated by abnormal mitral valve regurgitation (asterisks in E) and aortic regurgitation (AR, in F) at E15.5 and E17.5, respectively. Aortic flow (Ao); A wave, ventricular filling during atrial contraction (A); E wave, passive ventricular filling (E).

and thus retention of spindle symmetry [7, 8]. Further inspection of mitotic spindles revealed spindle misorientation. The spindle angle relative to the cell-substrate adhesion plane in ~80% of *Pcnt*$^{-/-}$ MEFs was >10°, whereas spindles in *Pcnt*$^{+/+}$ MEFs were largely (~50%) parallel to the substratum (0°) (Figures 2A, 2B, and S3A). Importantly, spindle misorientation (Figures 2E, 2F, and S3B) and diminished astral MTs (Figures 2G and 2H) were also identified in all three MOPDII skin fibroblast lines examined, strengthening the idea that spindle misorientation is a conserved phenotype of Pcnt deficiency in both organisms and is likely a contributing factor to the pathogenic mechanisms of MOPDII.

To explore the molecular mechanism of spindle misorientation in *Pcnt*-deficient cells, we screened known centrosomal proteins for changes in localization by immunofluorescence (~30 proteins tested). We unexpectedly identified a subset of proteins (Cep215/Cdk5rap2/hCnn, ninein, centriolin) that showed near-complete (up to 99.35%) loss from spindle poles in the absence of Pcnt (Figures 3A, 3D, and S3C–S3E). Total levels of Cep215 and ninein in cell lysates were unaffected

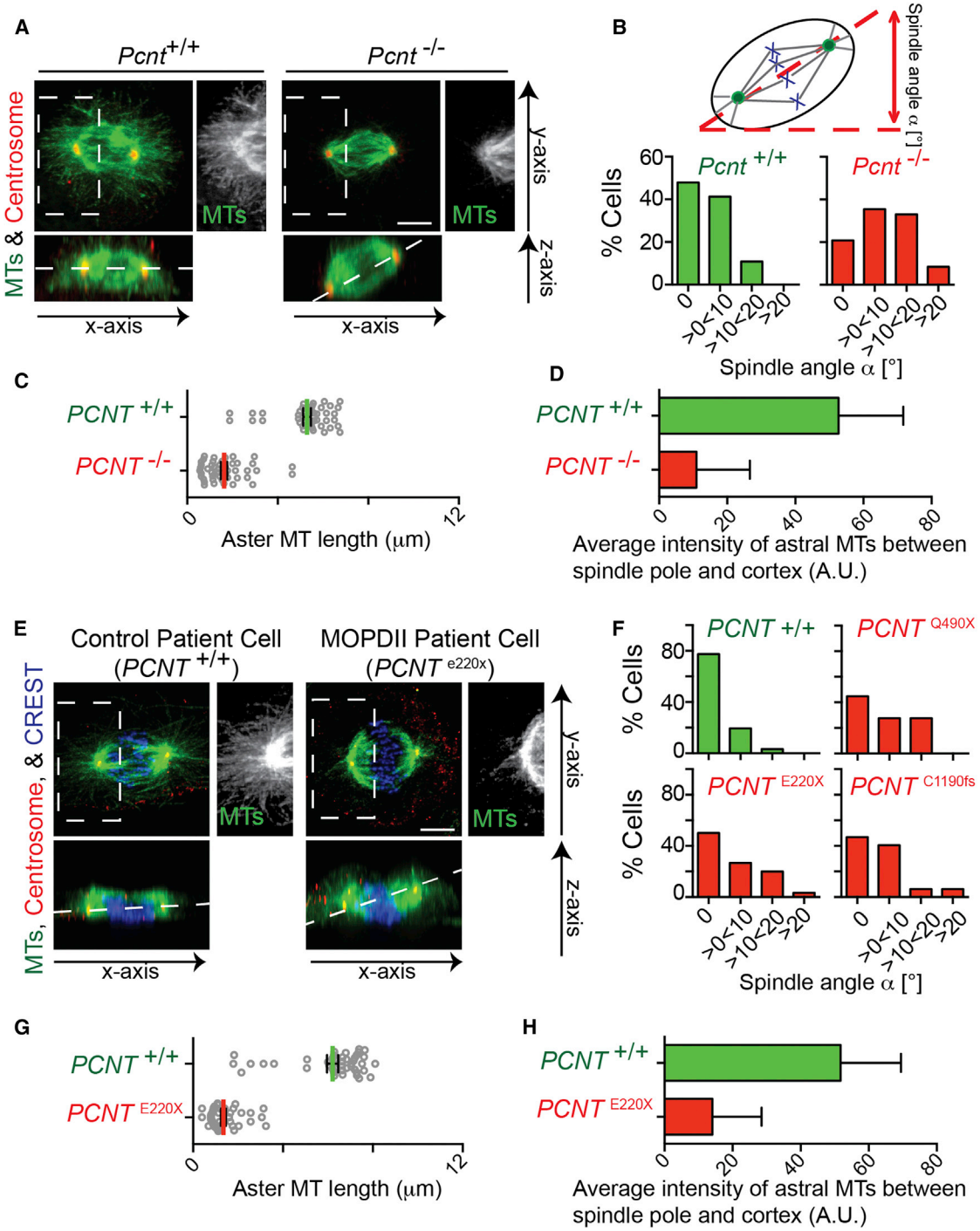

Figure 2. Spindle Misorientation in Both Primary *Pcnt*$^{-/-}$ MEFs and Cultured Pcnt-Deficient MOPDII Patient Cells

(A) Spindle angle, angles between dashed lines (lower panels; x/z-axis projections) and the substratum. Top panels: maximal projections of z-axis; MTs, green (α-tubulin); centrosomes, red (γ-tubulin). Insets show the lack of astral MTs in *Pcnt*$^{-/-}$ MEFs compared to control.

(B) Quantification of (A) showing a significant increase (>0°) of spindle angle in *Pcnt*$^{-/-}$ MEFs (n > 45 cells for *Pcnt*$^{+/+}$ and *Pcnt*$^{-/-}$; p < 0.0002; individual scatter plots for each angle shown in Figure S3A.

(C and D) Quantification of astral MT length and average intensity of astral MTs between spindle pole and cortex (n > 50 asters per treatment, p < 0.001).

(E) x/y and x/z axis projections of control and Pcnt-deficient MOPDII patient fibroblasts (*PCNT*^{e220x}) are shown. MTs, green (α-tubulin); centrosomes, red (5051); kinetochores, blue (CREST). Insets show diminished astral MTs in Pcnt-deficient cells compared to control.

(F) A significant increase in misoriented spindles is observed in Pcnt-deficient MOPDII fibroblasts (red; *PCNT*^{Q490X}, *PCNT*^{E220X}, and *PCNT*^{C1190fs}) versus control patients (green; *PCNT*$^{+/+}$). A total of 29–32 spindles were analyzed for each group; p values compared to control: 0.0034 (*PCNT*^{Q490X}), 0.011 (*PCNT*^{E220X}), 0.0166 (*PCNT*^{C1190fs}). Individual scatter plot for each angle is shown in Figure S3B.

(G and H) Astral MT length (G) and average intensity (H) of astral MTs quantified between spindle pole and cortex (n > 50 asters per treatment, p < 0.001). Error bars were calculated using SE over at least n = 3 experiments.

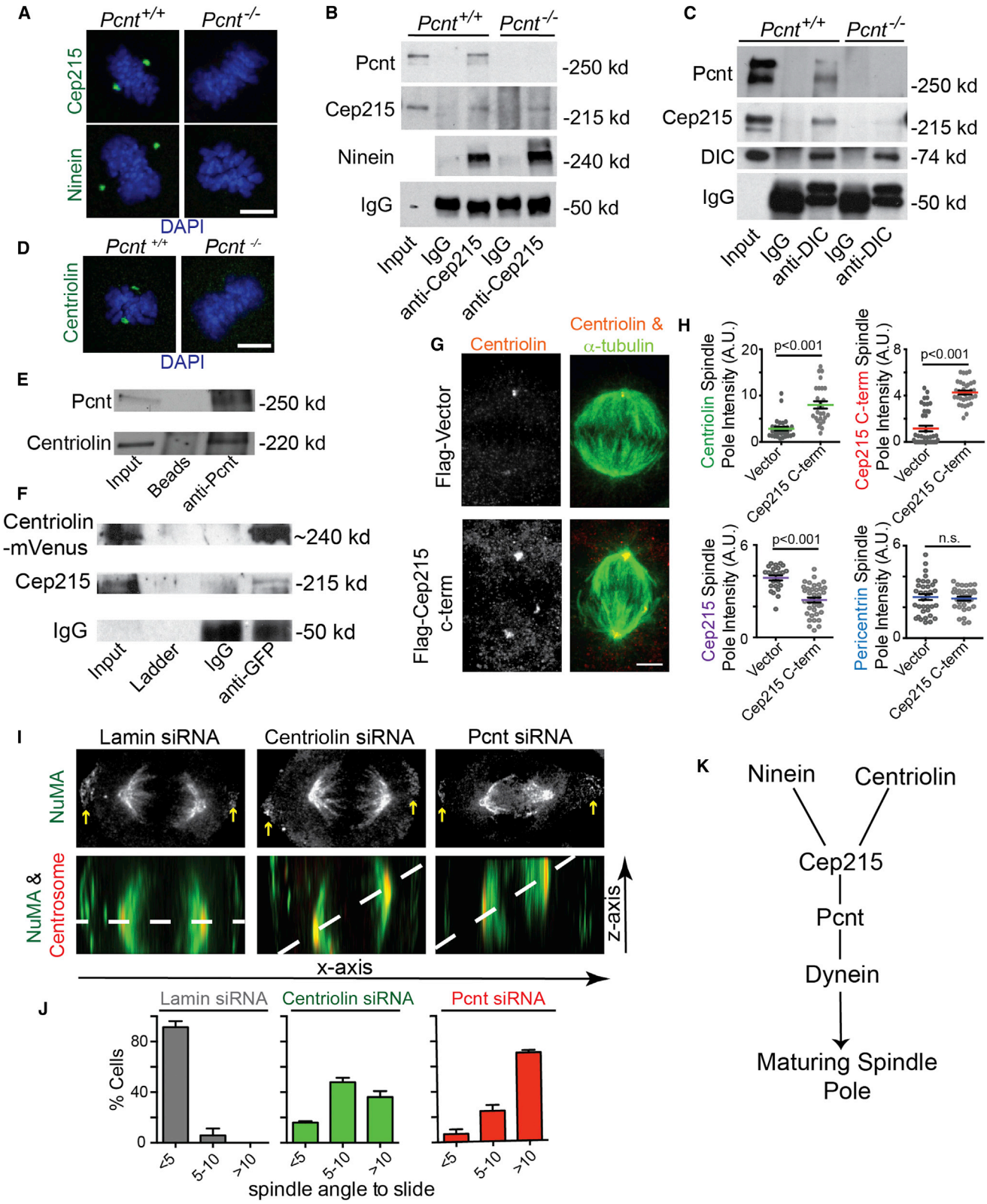

Figure 3. Pcnt Interacts with Centriolin, Cep215, and Ninein, Is Required for Their Localization to the Mitotic Spindle Poles, and Contributes to Spindle Orientation

(A) Ninein and Cep215 (green) are significantly displaced from mitotic spindle poles in *Pcnt*$^{-/-}$ MEFs compared to *Pcnt*$^{+/+}$ MEFs. DNA, blue. Scale bar represents 5 μm. Quantification in Figure S3D.

(B and C) Immunoprecipitation from *Pcnt*$^{+/+}$ MEFs compared to *Pcnt*$^{-/-}$ MEFs reveals protein complexes: Pcnt and Cep215 (B; also see in Figures S3G and S3H); Cep215 and ninein (B); Dynein, Cep215, and Pcnt (C).

(legend continued on next page)

(Figures S1C and S3F), suggesting a model in which Pcnt is required to localize ninein and Cep215 to spindle poles. Indeed, ninein and Cep215 localized to mitotic spindle poles (Figure 3A) as well as motile pericentriolar satellites (Figure S3C). Similar to Pcnt, these two proteins have roles in MT organization and anchoring at centrosomes/spindle poles [11–13]. Moreover, mutation of Cep215 or its fly homolog (Cnn) cause spindle misorientation [14, 15], due to disruption of astral MTs [16].

The requirement for Pcnt in localizing Cep215 and ninein to centrosomes/spindle poles suggested that they might form protein complexes. Immunoprecipitation from cell lysates demonstrated novel interactions between Pcnt and ninein, as well as ninein and Cep215, and confirmed a previously identified interaction between Pcnt and Cep215 (Figures 3B, S3G, and S3H) [12, 17]. Intriguingly, our results also showed that in the absence of Pcnt, ninein and Cep215 still coprecipitated (Figures 3B and S3G), suggesting that they formed a subcomplex. Using a previously identified Cep215-binding domain of Pcnt (PcntB7, aa 1801–2100) [18], we found that when expressed in *Pcnt*$^{-/-}$ MEFs, spindle misorientation was diminished (Figures S3J and S3K). Furthermore, this Pcnt fragment rescued localization of Cep215 to spindle poles in *Pcnt*$^{-/-}$ MEFs compared to mock-transfected *Pcnt*$^{-/-}$ MEFs (Figures S3L and S3M), suggesting that the spindle association of Cep215 through Pcnt is crucial for spindle orientation. Together, these studies reveal a novel multimolecular Pcnt complex(es) and implicate these associated components in spindle orientation.

Pcnt is known to interact with dynein [19, 20], so we tested whether the Pcnt-interacting proteins Cep215 and ninein also interacted with dynein. We found that dynein and Cep215 coprecipitated in a Pcnt-dependent manner (Figure 3C). Using a siRNA-targeted-depletion-based approach, we characterized the nature of the interaction between ninein, Cep215, and Pcnt at spindle poles. Strikingly, neither Cep215 nor Pcnt required ninein for spindle pole localization (Figure S3I), suggesting that Pcnt and Cep215 anchor ninein at the mitotic spindle pole (Figures 3A, 3B, and S3G–S3I) and likely get there through dynein-mediated transport (Figure 3C, modeled in Figure 3K). This result, together with the Pcnt-independent interaction between Cep215 and ninein (Figures 3B, S3G, and S3H), suggested that a complex of pericentrin, ninein, and Cep215 interacted with dynein through Pcnt. We propose that the association with dynein is required for this complex to target to spindle poles, as shown for Pcnt, Cep215, and γ-tubulin (modeled in Figure 3K) [20, 21]. Consistent with this idea was the localization of Pcnt-interacting proteins to pericentriolar satellites (Figure S3C), assemblies of centrosome proteins carried by dynein to centrosomes [20–22].

The third protein identified in our screen, centriolin [9, 18], was essentially undetectable at spindle poles upon Pcnt loss (Figures 3D and S3E), suggesting Pcnt anchoring. Centriolin levels were slightly diminished in *Pcnt*$^{-/-}$ cells (unlike Cep215 and ninein), but this minimal depletion could not account for the significant centriolin loss from poles (Figure S4A). We demonstrated that centriolin coimmunoprecipitated with Pcnt (Figures 3E and S4B) and Cep215 (Figure 3F). We took advantage of the previously identified Pcnt-interacting domain of Cep215 (Cep215 C-term, aa 1201–1822) [10] and tested whether this domain affected the spindle pole localization of centriolin (Figures 3G and 3H). Cep215 C-term localized robustly to mitotic spindle poles (Figures 3H), uncoupled pole localization of endogenous Cep215 (Figure 3H), and was accompanied by a 2-fold increase in the spindle pole localization of centriolin (Figures 3G and 3H). Pcnt intensity at mitotic spindle poles was unchanged with Cep215 C-term expression, suggesting that Pcnt is upstream of Cep215 recruitment at poles (Figure 3H, modeled in Figure 3K).

Since centriolin has never been implicated in spindle orientation, we compared human epithelial cells depleted of centriolin or Pcnt to controls (lamin siRNA) using previously published siRNAs [9, 23] (Figure S4C). We found that centriolin depletion increased spindle misorientation to a level similar to Pcnt-depleted cells (Figures 3I and 3J). Also similar to Pcnt-deficient cells (Figure 2), centriolin-depleted cells showed a decrease in overall astral MT length and number (Figure S4D), strengthening the idea that the novel mitotic roles of centriolin are functionally linked with Pcnt.

To clarify the potential interplay between the centrosome-localized Pcnt-associated complex for spindle orientation, we compared it to the classical spindle orientation complex located at the cell cortex (NuMA, aPKC, p150^{glued}). We found that it remained intact at the cell cortex (Figures 3I, S4E, and S4F), suggesting that the cortical NuMA pathway for spindle symmetry/orientation [24] was not responsible for the observed phenotypes with Pcnt or Centriolin loss. Our observations suggest a spindle-pole-anchored complex where Pcnt recruits Cep215, which, in turn, recruits centriolin and/or ninein (Figure 3K). This centrosome-based complex would be required for modulating orientation of the spindle and thus, the cell division plane.

To test whether spindle misorientation occurred in vivo and potentially contributed to MOPDII pathogenesis, we focused on the organs exhibiting the most dramatic phenotypes,

(D) *Pcnt*$^{-/-}$ MEFs show significant displacement of centriolin (green) from mitotic spindle poles compared to *Pcnt*$^{+/+}$ MEFs. DNA, blue. Scale bar represents 5 μm.

(E and F) Immunoprecipitation from human epithelial cells demonstrates an interaction between Pcnt and centriolin (E, reciprocal immunoprecipitation in Figure S4B). An interaction was observed in cells stably expressing Centriolin-mVenus [9] and Cep215 (F).

(G and H) Cells expressing Cep215 C-term (C-term; aa 1201–1822; reported in [10]) have an increase in Centriolin recruitment to spindle poles that was comparable to the increased recruitment of the C terminus of Cep215 ($p < 0.001$ as marked, n.s. is nonsignificant, representative of three experiments). A loss of endogenous Cep215 at the spindle pole was observed using an antibody targeting the Cep215 N-terminal domain. No effect was observed on Pcnt localization when Cep215 C-term was expressed.

(I) Centriolin- or Pcnt-depleted cells show increased spindle misorientation. Shown are maximum projections of z-axis; centrosome (5051, red), NuMA (green). Note that NuMA localization is unaffected at both spindle poles and cell cortex (yellow arrows, x/y axis maximum projection).

(J) Quantification showing a significant increase (>5°) of spindle angle in cells depleted of either centriolin or Pcnt (~3-fold, n = 3 experiments, $p < 0.001$ comparing spindle angles >5° across treatments. n > 20 cells counted/experiment).

(K) Model represents a Pcnt-mediated interaction between Cep215 and dynein (as demonstrated by immunoprecipitation in C) and Ninein interacting peripherally with Cep215 (shown both by immunoprecipitation in B and Figure S3G, and genetically in S3I). Pcnt-anchored Cep215 further interacts with Centriolin (E and F) through the C-terminal domain of Cep215 (G and H).

Error bars were calculated using SE over at least n = 3 experiments.

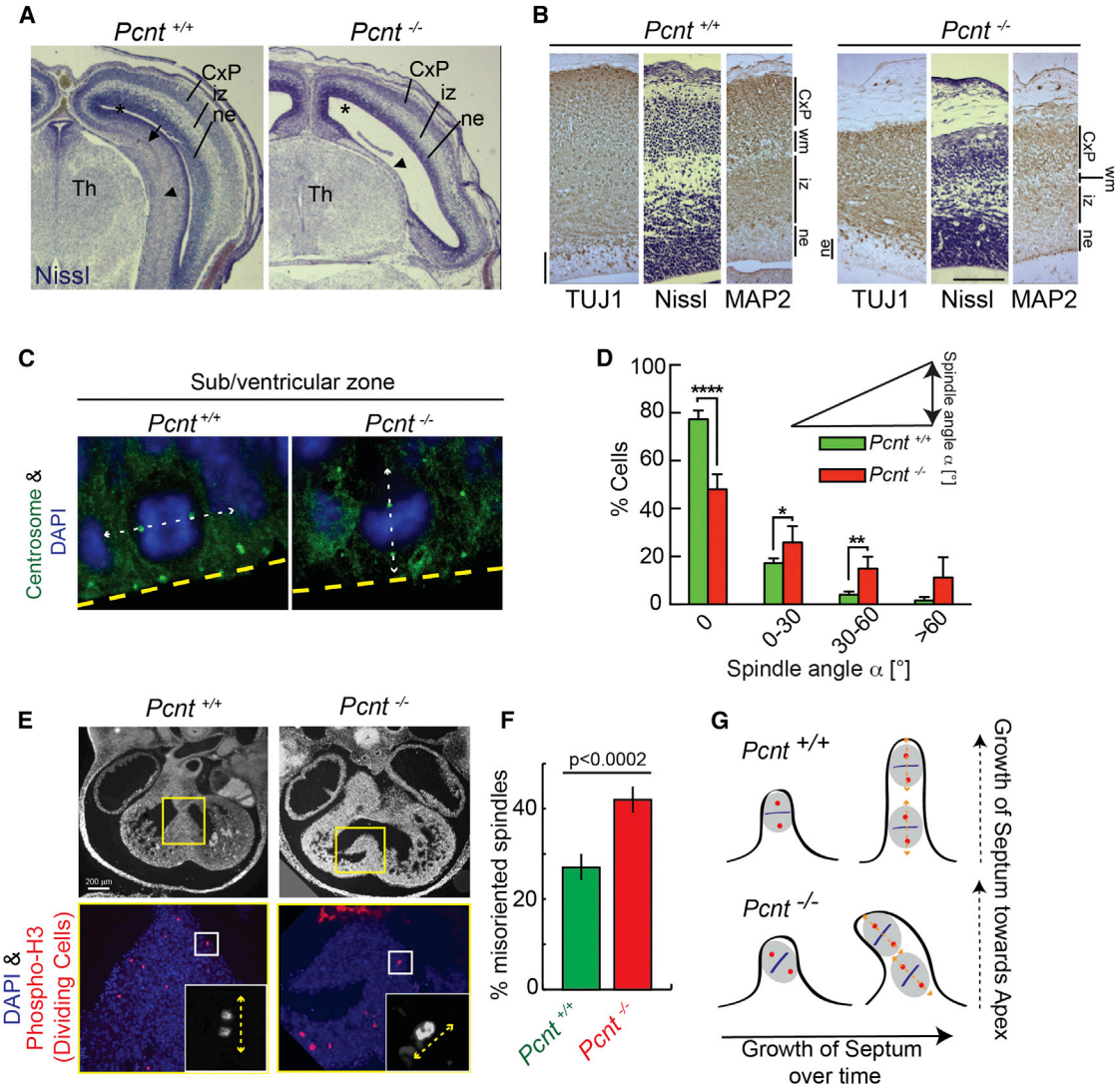

Figure 4. Asymmetric Spindles and Misoriented Divisions Are Significantly Increased in Microcephalic Brains and Developing Hearts of *Pcnt*$^{-/-}$ Mice

(A) Coronal forebrain sections reveal defective brain development and enlarged ventricles (*) in *Pcnt*$^{-/-}$ mice from E17 littermates (Nissl staining). Note severe dysplasia of hippocampus compared to control (arrow) and medial temporal cortex (arrowheads) in *Pcnt*$^{-/-}$ mice.

(B) An enlargement from a portion in (A) demonstrates Nissl staining and staining for MAP2 (phenotypic marker for differentiated neurons) and TUJ1 (neuron-specific class III β-tubulin) to determine neuronal differentiation. In *Pcnt*$^{-/-}$ section, note thinning of the cortical plate (CxP); a significant decrease in the development of interstitial zones (iz), neuroepithelium (ne), and future white matter (wm); and reduced levels of MAP2 and TUJ1. Scale bar represents 100 μm.

(C) Shown are single mitotic cells localized at the ventricular zone (VZ) from E13.5 *Pcnt*$^{+/+}$ and *Pcnt*$^{-/-}$ littermates. Sections were stained for γ-tubulin to label mitotic spindle poles. White dashed lines depict the cell division axis and a yellow dashed line identifies the ventricular lining. DAPI (DNA, blue).

(D) Compared to age-matched *Pcnt*$^{+/+}$ embryos (n = 4), *Pcnt*$^{-/-}$ embryos showed a significant increase in asymmetric divisions at the ventricular zone (E13.5, n = 5; ****p < 0.0001, **p < 0.01, *p < 0.05; n > 250 cells).

(E and F) Cell division axis within the developing atrial septum of *Pcnt*$^{-/-}$ embryos is significantly misdirected compared to *Pcnt*$^{+/+}$ embryos (E12.5; n = 4 to 5 embryos for each genotype, quantification in F). Top in (E), in utero ultrasound image demonstrating misdirected septal development in *Pcnt*$^{-/-}$ embryo compared to *Pcnt*$^{+/+}$ embryo. Bottom, enlarged view of boxed region in ultrasound was stained for phospho-H3 (red) to specifically label dividing cells. Inset shows a dividing cell with dashed lines depicting the cell division axis. Scale bar in (E) represents 200 μm.

(G) Shown is a schematic for measuring spindle misorientation in a developing atrial septum. Spindle angles (orange dotted line) were measured in relation to the axis perpendicular to the septum base (black dotted line). The septum grows toward the apex of the heart through symmetric divisions over time. When division axis becomes predominantly asymmetric, we propose that the septum is more likely to grow in an unpolarized way (as seen in E).

Error bars were calculated using SE over at least n = 3 experiments.

namely the brain, heart, and kidney (data not shown). The small brains of *Pcnt*$^{-/-}$ mice showed enlarged cerebral ventricles and thinning of the cerebral cortex, particularly the cortical plate, which harbors young neurons at this stage (Figures 4A and 4B; n = 5/5). The phenotypic marker for differentiated neurons (MAP2) was expressed at low levels in *Pcnt*$^{-/-}$ mouse cortex (Figure 4B; n = 3/3) and hippocampus (data not shown), suggesting a delay in neuronal differentiation and/or defects in neurogenesis. Indeed, neuron-specific TUJ1 staining was reduced in the neuroepithelium (ne) where nascent neurons

arise (Figure 4B; n = 3/3, E17), demonstrating that neurogenesis and the earliest phases of neuronal differentiation were compromised, a condition known to lead to microcephaly [25]. Further examination of the brain ventricular zone (E13.5) showed a significant increase in asymmetric divisions (Figures 4C and 4D) compared to wild-type controls. Increased asymmetric divisions or aberrant proliferative/symmetric divisions [26] in this area of the brain are associated with microcephaly and can be caused by mutations in other centrosome genes [25, 27–29].

Similar to microcephalic brains, mouse hearts in *Pcnt*$^{-/-}$ mice showed significantly more misoriented divisions compared to normal littermates. This was particularly striking in the developing cardiac septum and occurred concomitantly with misdirected growth of the septum (Figures 4E and 4F, modeled in 4G). These results indicate that orientated division through the spindle pole component Pcnt in vivo is crucial for proper organogenesis. The aberrant orientation of spindles and plane of cell division in the absence of Pcnt in mice is likely to contribute to anatomic developmental abnormalities in the same and perhaps other organs in MOPDII.

Our molecular model for spindle misorientation in *Pcnt*$^{-/-}$ mice involves a novel Pcnt protein complex comprised of key centrosome/spindle pole components that assemble onto spindle poles in a dynein-dependent manner to control astral MT organization at this site. In the absence of Pcnt, these proteins are lost from spindle poles, diminishing the efficacy of astral MT assembly, which is required for proper spindle orientation. Spindle misorientation in *Pcnt*$^{-/-}$ mice and MOPDII cells provides plausible mechanisms for (1) cardiac septation defects, through misdirected growth of septa; (2) microcephaly, through decreased proliferative symmetric divisions, which are required to populate neural stem cells for brain growth; and (3) cystic kidneys (not shown) through division in the plane of the lumen, increasing its diameter. At a global level, aberrant divisions could affect stem cells and create more differentiated cells at the expense of self-renewing divisions [30], decreasing cell numbers in many, if not all, organs. This could account for small brain, body, and organ size of *Pcnt*$^{-/-}$ mice and MOPDII individuals, as seen in microcephalies caused by mutations in other centrosome genes [14, 28, 29].

Taken together, the unique subset of Pcnt-interacting proteins may collectively define a spindle-pole-based complex for spindle orientation. The genetic association of mutant *ninein* (*NIN*) and *Cep215* (*CEP215*) with microcephaly [27, 31] supports the idea that these proteins contribute to the phenotypes in MOPDII and the *Pcnt*$^{-/-}$ mouse through their loss from spindle poles in the absence of Pcnt. These results suggest that Pcnt may act as the core scaffold for such a complex during embryonic development. It is unclear why mutation of some centrosome genes disrupts a single organ, whereas Pcnt mutations affect many organs.

This work shows for the first time that *Pcnt*$^{-/-}$ mice exhibit pathology similar to and beyond those of MOPDII. We believe that the prenatal lethality of the *Pcnt*$^{-/-}$ mouse is an excellent model for the human condition. Like *Pcnt*$^{-/-}$ mice, MOPDII is an extremely rare human disorder. This is likely due to the fact that many human embryos and fetuses do not progress to birth. In addition, many of those that are born weigh only 1–2 pounds at birth and often do not develop beyond this stage. Inbred *Pcnt*$^{-/-}$ mice avoid confounding effects of genetic heterogeneity in patients and show that Pcnt deficiency alone can cause a phenotype continuum spanning MOPDII. In addition, variable phenotypes occur between *Pcnt*$^{-/-}$ mice from the same litter as seen in MOPDII patients. These may result from genetic modifier effects, which would allow long-term survival of some MOPDII patients. Severe cardiovascular defects in *Pcnt*$^{-/-}$ embryos are not expected in MOPDII patients, as such defects would be prenatal lethal. However, it is interesting that both *Pcnt*$^{-/-}$ mice and MOPDII individuals die of cardiovascular issues, albeit at different stages of development. These defects are informative regarding developmental processes that may be impacted by Pcnt deficiency. The *Pcnt*$^{-/-}$ mouse model also reveals unique phenotypes not reported thus far in the human conditions (polydactyly, anopthalmia) (Figure S2), which could be species specific, reflect different gene-environment interactions, or result from the role of Pcnt in cilia integrity/signaling [23, 32], although this was not clearly identified in *Pcnt*$^{-/-}$ mice. Alternatively, these additional phenotypes may suggest higher risks for such developmental anomalies in MOPDII patients and even their families. Thus, our Pcnt mouse model provides insights into the etiology and broad defects in MOPDII.

Supplemental Information

Supplemental Information includes four figures, one table, and Supplemental Experimental Procedures and can be found with this article online at http://dx.doi.org/10.1016/j.cub.2014.08.029.

Author Contributions

C.-T.C. designed and performed experiments featured in Figures 3 and 4; H.H. contributed to Figures 2 and 3; and Q.Y. contributed to Figures 1 and 4. C.-T.C. and H.H. worked on all written versions of manuscript.

Acknowledgments

The article is dedicated to the memory of C.-T.C., a thoughtful, innovative, and energetic scientist, and most importantly our dear friend. Ting spearheaded a major part of the work presented herein and he will be truly missed among his peers. S.D. is supported by NIH RO1-GM051994-14, C.L. is supported by NIH U01-HL098180-05, and H.H. is supported by NIH K99-GM107355. We thank Stephen Jones and the UMMS Transgenic Animal Modeling Core, Paul Furcinitti of the UMMS Digital Light Microscopy, Yu Liu of the UMMS DERC Morphology Core, and James Fitzpatrick of the Waitt Advanced Biophotonics Center at Salk institutes.

Received: March 26, 2014
Revised: July 15, 2014
Accepted: August 13, 2014
Published: September 11, 2014

References

1. Delaval, B., and Doxsey, S.J. (2010). Pericentrin in cellular function and disease. J. Cell Biol. *188*, 181–190.
2. Rauch, A., Thiel, C.T., Schindler, D., Wick, U., Crow, Y.J., Ekici, A.B., van Essen, A.J., Goecke, T.O., Al-Gazali, L., Chrzanowska, K.H., et al. (2008). Mutations in the pericentrin (PCNT) gene cause primordial dwarfism. Science *319*, 816–819.
3. Hall, J.G., Flora, C., Scott, C.I., Jr., Pauli, R.M., and Tanaka, K.I. (2004). Majewski osteodysplastic primordial dwarfism type II (MOPD II): natural history and clinical findings. Am. J. Med. Genet. A. *130A*, 55–72.
4. Majewski, F., Ranke, M., and Schinzel, A. (1982). Studies of microcephalic primordial dwarfism II: the osteodysplastic type II of primordial dwarfism. Am. J. Med. Genet. *12*, 23–35.
5. Bober, M.B., Khan, N., Kaplan, J., Lewis, K., Feinstein, J.A., Scott, C.I., Jr., and Steinberg, G.K. (2010). Majewski osteodysplastic primordial dwarfism type II (MOPD II): expanding the vascular phenotype. Am. J. Med. Genet. A. *152A*, 960–965.

6. Ucar, B., Kilic, Z., Dinleyici, E.C., Yakut, A., and Dogruel, N. (2004). Seckel syndrome associated with atrioventricular canal defect: a case report. Clin. Dysmorphol. *13*, 53–55.
7. Delaval, B., Bright, A., Lawson, N.D., and Doxsey, S. (2011). The cilia protein IFT88 is required for spindle orientation in mitosis. Nat. Cell Biol. *13*, 461–468.
8. Hehnly, H., and Doxsey, S. (2014). Rab11 endosomes contribute to mitotic spindle organization and orientation. Dev. Cell *28*, 497–507.
9. Hehnly, H., Chen, C.-T., Powers, C.M., Liu, H.-L., and Doxsey, S. (2012). The centrosome regulates the Rab11- dependent recycling endosome pathway at appendages of the mother centriole. Curr. Biol. *22*, 1944–1950.
10. Buchman, J.J., Tseng, H.-C., Zhou, Y., Frank, C.L., Xie, Z., and Tsai, L.-H. (2010). Cdk5rap2 interacts with pericentrin to maintain the neural progenitor pool in the developing neocortex. Neuron *66*, 386–402.
11. Kim, S., and Rhee, K. (2014). Importance of the CEP215-pericentrin interaction for centrosome maturation during mitosis. PLoS ONE *9*, e87016.
12. Haren, L., Stearns, T., and Lüders, J. (2009). Plk1-dependent recruitment of gamma-tubulin complexes to mitotic centrosomes involves multiple PCM components. PLoS ONE *4*, e5976.
13. Logarinho, E., Maffini, S., Barisic, M., Marques, A., Toso, A., Meraldi, P., and Maiato, H. (2012). CLASPs prevent irreversible multipolarity by ensuring spindle-pole resistance to traction forces during chromosome alignment. Nat. Cell Biol. *14*, 295–303.
14. Lizarraga, S.B., Margossian, S.P., Harris, M.H., Campagna, D.R., Han, A.-P., Blevins, S., Mudbhary, R., Barker, J.E., Walsh, C.A., and Fleming, M.D. (2010). Cdk5rap2 regulates centrosome function and chromosome segregation in neuronal progenitors. Development *137*, 1907–1917.
15. Yamashita, Y.M., Mahowald, A.P., Perlin, J.R., and Fuller, M.T. (2007). Asymmetric inheritance of mother versus daughter centrosome in stem cell division. Science *315*, 518–521.
16. Megraw, T.L., Kao, L.R., and Kaufman, T.C. (2001). Zygotic development without functional mitotic centrosomes. Curr. Biol. *11*, 116–120.
17. Hubner, N.C., Bird, A.W., Cox, J., Splettstoesser, B., Bandilla, P., Poser, I., Hyman, A., and Mann, M. (2010). Quantitative proteomics combined with BAC TransgeneOmics reveals in vivo protein interactions. J. Cell Biol. *189*, 739–754.
18. Gromley, A., Jurczyk, A., Sillibourne, J., Halilovic, E., Mogensen, M., Groisman, I., Blomberg, M., and Doxsey, S. (2003). A novel human protein of the maternal centriole is required for the final stages of cytokinesis and entry into S phase. J. Cell Biol. *161*, 535–545.
19. Purohit, A., Tynan, S.H., Vallee, R., and Doxsey, S.J. (1999). Direct interaction of pericentrin with cytoplasmic dynein light intermediate chain contributes to mitotic spindle organization. J. Cell Biol. *147*, 481–492.
20. Young, A., Dictenberg, J.B., Purohit, A., Tuft, R., and Doxsey, S.J. (2000). Cytoplasmic dynein-mediated assembly of pericentrin and gamma tubulin onto centrosomes. Mol. Biol. Cell *11*, 2047–2056.
21. Jia, Y., Fong, K.-W., Choi, Y.-K., See, S.-S., and Qi, R.Z. (2013). Dynamic recruitment of CDK5RAP2 to centrosomes requires its association with dynein. PLoS ONE *8*, e68523.
22. Kubo, A., Sasaki, H., Yuba-Kubo, A., Tsukita, S., and Shiina, N. (1999). Centriolar satellites: molecular characterization, ATP-dependent movement toward centrioles and possible involvement in ciliogenesis. J. Cell Biol. *147*, 969–980.
23. Mikule, K., Delaval, B., Kaldis, P., Jurcyzk, A., Hergert, P., and Doxsey, S. (2007). Loss of centrosome integrity induces p38-p53-p21-dependent G1-S arrest. Nat. Cell Biol. *9*, 160–170.
24. Mapelli, M., and Gonzalez, C. (2012). On the inscrutable role of Inscuteable: structural basis and functional implications for the competitive binding of NuMA and Inscuteable to LGN. Open Biol *2*, 120102.
25. Thornton, G.K., and Woods, C.G. (2009). Primary microcephaly: do all roads lead to Rome? Trends Genet. *25*, 501–510.
26. Gillies, T.E., and Cabernard, C. (2011). Cell division orientation in animals. Curr. Biol. *21*, R599–R609.
27. Tan, C.A., Topper, S., Ward Melver, C., Stein, J., Reeder, A., Arndt, K., and Das, S. (2014). The first case of CDK5RAP2-related primary microcephaly in a non-consanguineous patient identified by next generation sequencing. Brain Dev. *36*, 351–355.
28. Fish, J.L., Kosodo, Y., Enard, W., Pääbo, S., and Huttner, W.B. (2006). Aspm specifically maintains symmetric proliferative divisions of neuroepithelial cells. Proc. Natl. Acad. Sci. USA *103*, 10438–10443.
29. Gruber, R., Zhou, Z., Sukchev, M., Joerss, T., Frappart, P.-O., and Wang, Z.-Q. (2011). MCPH1 regulates the neuroprogenitor division mode by coupling the centrosomal cycle with mitotic entry through the Chk1-Cdc25 pathway. Nat. Cell Biol. *13*, 1325–1334.
30. Neumüller, R.A., and Knoblich, J.A. (2009). Dividing cellular asymmetry: asymmetric cell division and its implications for stem cells and cancer. Genes Dev. *23*, 2675–2699.
31. Dauber, A., Lafranchi, S.H., Maliga, Z., Lui, J.C., Moon, J.E., McDeed, C., Henke, K., Zonana, J., Kingman, G.A., Pers, T.H., et al. (2012). Novel microcephalic primordial dwarfism disorder associated with variants in the centrosomal protein ninein. J. Clin. Endocrinol. Metab. *97*, E2140–E2151.
32. Quinlan, R.J., Tobin, J.L., and Beales, P.L. (2008). Modeling ciliopathies: Primary cilia in development and disease. Curr. Top. Dev. Biol. *84*, 249–310.